Remote Sens. **2015**, *7*, 3088-3113; doi:10.3390/rs70303088

OPEN ACCESS

remote sensing

ISSN 2072-4292

www.mdpi.com/journal/remotesensing

Article

A Study of Coal Fire Propagation with Remotely Sensed Thermal Infrared Data

Hongyuan Huo [1,2,3], Zhuoya Ni [4,5], Caixia Gao [6], Enyu Zhao [3], Yuze Zhang [3], Yi Lian [1], Huili Zhang [7], Shiyue Zhang [1], Xiaoguang Jiang [3,8,9,*], Xianfeng Song [3], Ping Zhou [10] and Tiejun Cui [1]

1 College of Urban and Environmental Sciences, Tianjin Normal University, Tianjin 300387, China; E-Mails: hongyuanh@gmail.com (H.H.); fishlice@163.com (Y.L); seeyoaaa@hotmail.com (S.Z); tiejun_cui@163.com (T.C.)

2 Tianjin Engineering Center for Geospatial Information Technology, Tianjin 300387, China; E-Mail: song7537338@163.com

3 College of Resources and Environment, University of Chinese Academy of Sciences, Beijing 100049, China; E-Mails: zhaoenyusdu@163.com (E.Z.); zhangyuze999@126.com (Y.Z.)

4 School of Geography, Beijing Normal University, Beijing 100875, China; E-Mail: nizhuoya1987@163.com

5 ICube Lab, Université de Strasbourg, Boulevard Sebastien Brant, BP10413, Illkirch 67412, France

6 Academy of Opto-Electronics, Chinese Academy of Sciences, Beijing 100094, China; E-Mail: caixiagao2010@hotmail.com

7 Nanchang Institute of Technology, Jiangxi 330044, China; E-Mail: placugzhl@163.com

8 Key Laboratory of Quantitative Remote Sensing Information Technology, Academy of Opto-Electronics, Chinese Academy of Sciences, Beijing 100094, China

9 College of Geomatics and Geoinformation, Guilin University of Technology, Guilin 541004, China

10 College of Earth Sciences and Resources, China University of Geosciences, Beijing 100083, China; E-Mail: zhoupx@cugb.edu.cn

* Author to whom correspondence should be addressed; E-Mail: xgjiang@aoe.ac.cn; Tel.: +86-10-882-568-90; Fax: +86-10-882-561-45.

Academic Editors: Zhao-Liang Li, Jose A. Sobrino, Xiaoning Song and Prasad S. Thenkabail

Received: 9 November 2014 / Accepted: 15 February 2015 / Published: 17 March 2015

Abstract: Coal fires are a common and serious problem in most coal-bearing countries. Thus, it is very important to monitor changes in coal fires. Remote sensing provides a useful technique for investigating coal fields at a large scale and for detecting coal fires. In this

study, the spreading direction of a coal fire in the Wuda Coal Field (WCF), northwest China, was analyzed using multi-temporal Landsat Thematic Mapper (TM) and Enhanced Thematic Mapper (ETM+) thermal infrared (TIR) data. Using an automated method and based on the land surface temperatures (LST) that were retrieved from these thermal data, coal fires related to thermal anomalies were identified; the locations of these fires were validated using a coal fire map (CFM) that was developed via field surveys; and the cross-validation of the results was also carried out using the Advanced Spaceborne Thermal Emission and Reflection Radiometer (ASTER) thermal infrared images. Based on the results from longtime series of satellite TIR data set, the spreading directions of the coal fires were determined and the coal fire development on the scale of the entire coal field was predicted. The study delineated the spreading direction using the results of the coal fire dynamics analysis, and a coal fire spreading direction map was generated. The results showed that the coal fires primarily spread north or northeast in the central part of the WCF and south or southwest in the southern part of the WCF. In the northern part of the WCF, some coal fires were spreading north, perhaps coinciding with the orientation of the coal belt. Certain coal fires scattered in the northern and southern parts of the WCF were extending in bilateral directions. A quantitative analysis of the coal fires was also performed; the results indicate that the area of the coal fires increased an average of approximately 0.101 km^2 per year.

Keywords: coal fire detection; spreading direction; multi-temporal remote sensing; TM and ETM+

1. Introduction

Coal fires are defined as the spontaneous combustion of coal due to coal oxidation. Many researchers have noted that the ability to react with oxygen at ambient temperatures may be enhanced by the potential for coal spontaneous combustion [1,2]. Meanwhile, being accompanied by absorption of oxygen, this reaction takes an exothermic course, and it may increase the so-called "threshold" temperature that lies somewhere between 230 °C and 280 °C. At that point, the coal reaches its ignition or flash point and starts to burn, resulting in these coal fires [1,3].

Surface and underground coal fires have received great attention from researchers due to the threats they pose to non-renewable resources, local environment and regional climate. These uncontrolled fires are a common problem and are widely reported from most coal-bearing countries of the world, such as the USA, China, India, Australia, Russia, South Africa and Indonesia, among others (see Figure 1) [4–17]. For China, which is the world's largest coal-producing and coal-consuming country, approximately 10–200 Mt of coal reserves are consumed or made inaccessible for further mining operations due to coal fires (see Figure 2) [18,19]. In addition to the obvious economic losses of the waste of valuable coal resources, these coal fires have also led to health risks and environmental damages for the affected regions [15,20–24].

The detection of the propagation of coal fire is helpful for predicting their development trends and may provide useful information for controlling and extinguishing coal fires. Knowing the coal fire's

spreading direction is valuable for predicting the potential expansion of the hazard that is caused by coal fires and provides local firefighters with critical information. Previous literature discussing the coal fire spreading direction has been based mostly on various physical methods, such as temperature measurement monitoring in boreholes and radon and aeromagnetic measurements [25–30].

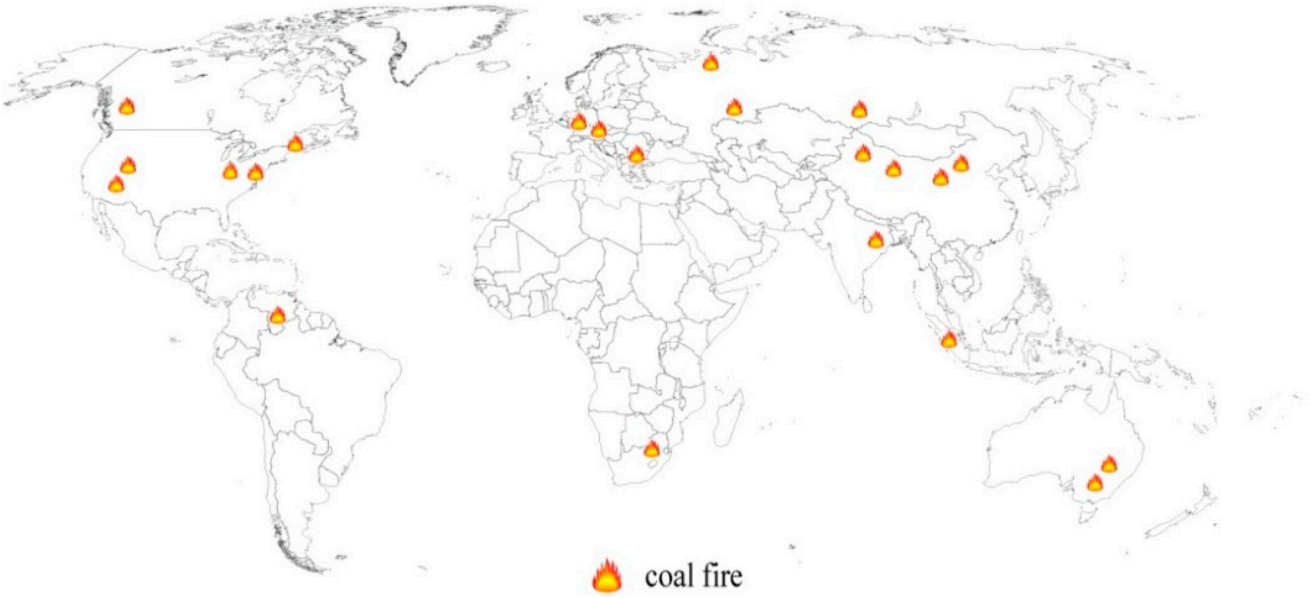

Figure 1. Global distribution of coal fires.

Remote sensing, as an advance technique and with a long history of application in the exploration of resources and environmental monitoring [31–41], has been used to investigate coal fires for nearly 5 decades [4,5,19,26,42–50]. Although aerial thermal scanners were used in previous studies, in the last two decades, studies of coal fire have focused on the use of thermal infrared data from satellites because these satellite thermal datasets can be used to retrieve the LST more precisely than ever with the help of multi-spectral channels in the thermal infrared region [37,51–53].

Various methods for detecting and monitoring coal seam fires using thermal infrared remotely sensed data have been developed. A density slicing method was successfully applied to extract coal fire information from Landsat-5 Thematic Mapper (TM) data [54–58]. Two complementary automated thermal anomaly extraction algorithms were presented to automatically delineate coal fire risk areas from multispectral satellite data and to automatically extract local coal-fire-related thermal anomalies from thermal Landsat TM and Enhanced Thematic Mapper (ETM+), Advanced Spaceborne Thermal Emission and Reflection Radiometer (ASTER) and Moderate-Resolution Imaging Spectroradiometer (MODIS) data [14]. The dual-band Dozier method [59] and the multi-temporal analysis method have been used by many researchers in recent years [20,57]. Other methods, such as the contextual method and fuel mask method, have also been used for coal fire detection [13].

Despite these above-mentioned important contributions, no substantial research has yet to study the coal fire spreading direction with long time series of satellite data. Considering the coarser spatial resolution of satellite data set such as the Advanced Very High Resolution Radiometer (AVHRR) and MODIS being not available for delineating some small coal fire spots, multi-temporal Landsat satellite thermal data and ASTER data with higher spatial resolution were used in this study to estimate these

coal fire spots that were not identified by them. In this study, an attempt was made to identify temperature anomalies across the Wuda Coal Field (WCF) to delineate the spatial distribution and spreading direction of the coal fires using the TIR remote sensing approach. The detection of the spreading direction of these coal fires will be helpful in predicting the velocity of coal fire expansion and the extent of coal fire development. These findings will be beneficial for coal mining activities and for enhancing the safety of miners. There have been numerous accidents that have been caused by coal fires that have claimed many victims, as discussed in the literature cited above [15,20–24]. Moreover, the detection of the spreading directions of coal fires will be useful to the local Coal Mine Bureau because available, precise information of this type may prove valuable in controlling and extinguishing these fires.

The period from 1999 to 2006 was selected for our study because coal seam fires began to expand more quickly during this time than before 1995, and because until 2006, mining activity was extensive, after which the surface of the WCF was devastated. The purpose of this study is to detect the natural principle of the coal fire spreading direction and its dynamics from 1999 to 2006. After 2007, many small coal fires were mainly caused by manual reasons, such as small mining activities. It is difficult to study the natural development and the corresponding spreading direction due to extensive mining activities and larger manual devastations to the WCF after 2007. From 1999 to 2006, the coal fires in the WCF were expanding naturally, and it is important to study the coal fires during this period of natural development without interference from human-induced factors so that the natural signals given off by the spread of the coal fires might be observed in the satellite remote-sensing images.

2. Study Area

The WCF is located in the Wuda district of Wuhai City, which is divided into three districts, namely the Wuda, Hainan and Haibowan districts (see Figure 2b), in the Inner Mongolia Autonomous Region in North China (see Figure 2a). Its geographic location extends latitudinally from 39°25′33″N to 39°35′41″N and longitudinally from 106°33′39″E to 106°54′17″E. Physically, the study area is bound by the Yellow River in the east, the Gobi Desert in the north and west, and Helan Mountain in the south, with a total area of approximately 35 km^2 (See Figure 2). The WCF includes three coal mining zones, namely Wuhushan, Suhaitu and Huangbaici, by the mining authority (See Figure 2c), which is approximately 10 km long (N-S) and 3–4 km wide (E-W), and its elevation ranges from 1100 to 1300 m above sea level. WCF mainly consists of bare rocks and soil and has a typical inland dry desert climate. Low rainfall amount (average annual precipitation ranges from 150 to 250 mm), massive evaporation and strong wind make this area very dry. In winter, it is very cold, and the temperature difference between day and night is very distinct.

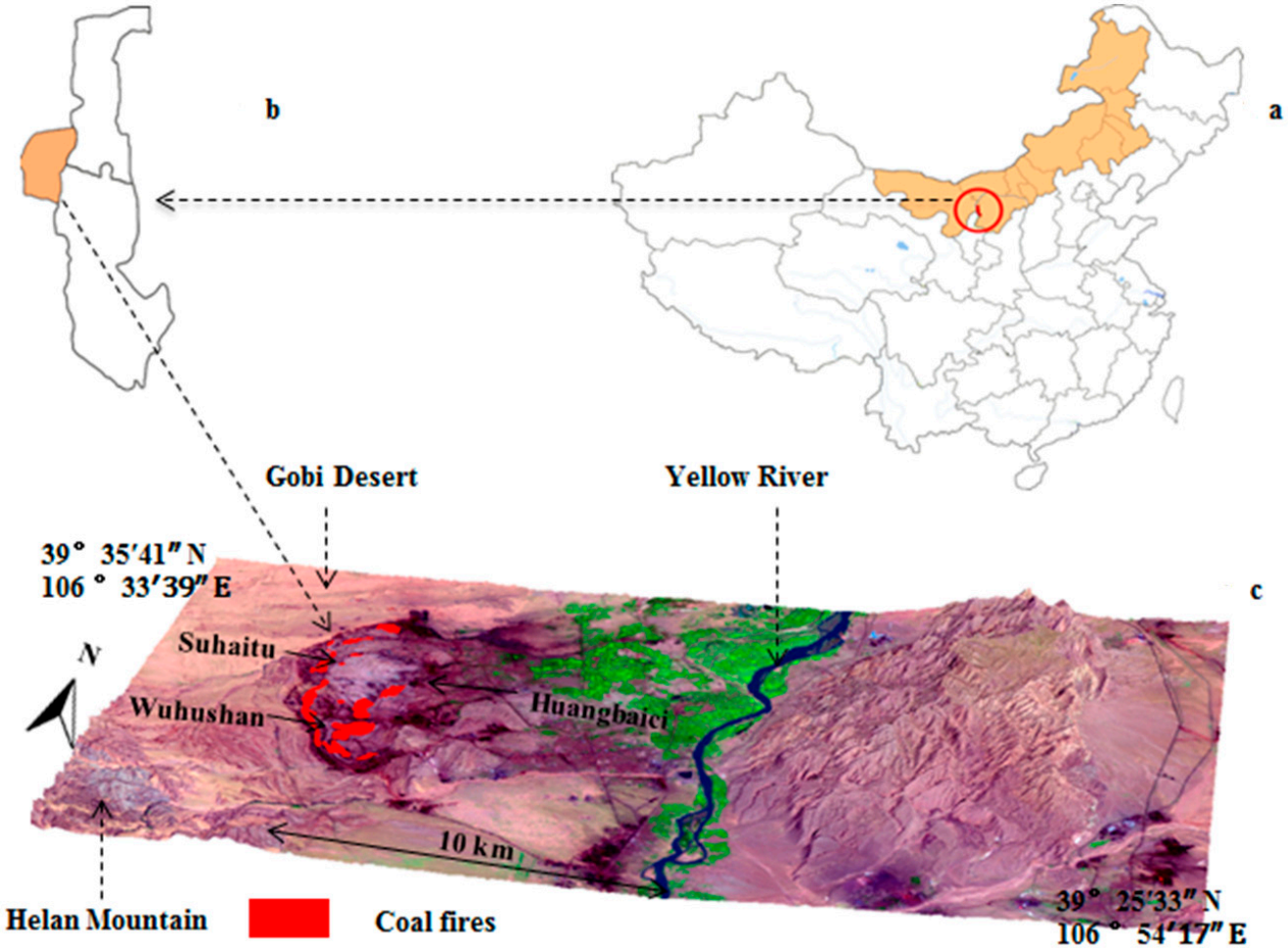

Figure 2. Study area of the Wuda Coal Field: (**a**) shows the location of the study area in Northwest China. (**b**) shows the WCF located in the Wuda district, Wuhai city; and (**c**) is a 3-D False Color Composite image (generated by coding ETM+7/4/2 in R/G/B) based on Landsat ETM+ data that were acquired on 30 August 2000, which is also integrated by coal fire map as investigated by the BRSC (Beijing Remote Sensing Com. Ltd, Beijing, China). (**c**) also shows the distribution of the three major local mines in WCF. Projection: UTM, zone 48 North, WGS 84.

3. Dataset and Pre-Processing

The satellite images that were used in this study were a series of multi-temporal Landsat TM/ETM+ thermal infrared images and ASTER data from 8 August 2001. During the data preprocessing, the summer or autumn cloud free images from 1999 to 2006 were collected and used, as listed in Table 1; these images were imported and converted to a WGS84 with UTM projection and zone 48 for the base projection. The ASTER imagery and ancillary data were also converted to the same projection for integrated analysis. To validate the results, the coal fire data that were extracted from the long time series Landsat TM/ETM+ images were all resampled to the same spatial resolution (90 m) as the ASTER data.

Table 1. Dataset used in this research. CFM: Coal Fire Map.

Data Type	Acquisition Time	Spatial Resolution
ETM+	12 August 1999	60 m
ETM+	30 August 2000	60 m
ETM+	4 October 2001	60 m
ETM+	20 August 2002	60 m
ETM+	3 May 2003	60 m
TM	17 August 2004	120 m
TM	7 August 2006	120 m
ASTER	8 August 2001	90 m
CFM	2002–2003	Scale: 1:5000

4. Methodology

The ETM+/TM band 6 data are useful in distinguishing gross thermal anomalies from the background of solar warming and can be used to map subsurface coal fires [60]. Using a series of multi-temporal ETM+/TM 6 images, we predicted the spreading direction of the underground coal fire. At first, using the single-window method [52,61], we retrieved the LSTs from the TM/ETM+ thermal data to extract the thermal-anomaly pixels from the background using a threshold technique. Second, using the ASTER data, the temperature images were retrieved in combination with a temperature/emissivity separation (TES) algorithm [62,63], and then, the LSTs that were derived from the ASTER data were used to cross-validate and test the availability of the LSTs from the Landsat TM/ETM+ band 6 thermal data. The official CFM that was produced by the field survey was used to validate the results that were obtained from the multi-temporal Landsat TM/ETM+ data. During the validation of the results, the 2001 ASTER datasets (with a spatial resolution of 90 m) were used in an attempt to perform a cross-validation analysis and show the degree of consistency of the results that were extracted from the two types of satellite data. The coal fires from the 2002–2003 Landsat data were validated using the CFM that was developed by the Wuda Local Mineral Bureau, which performed the field work beginning in 2002 and finished in 2003. Thus, the field survey data were available for only 2002 and 2003 and were also used to validate the results from the two years. Lastly, the coal fire spreading direction was delineated using coal fires that were extracted from a longtime series of satellite data set. Figure 3 shows a flow chart of the data pre-processing and analysis that were used in this study. This flow chart includes data acquisition, preprocessing, analysis, and use of the threshold technique in developing the coal fire map and validation of the results using the field survey findings.

4.1. LST Retrieval from ETM+/TM Band 6 TIR Data

The first step was to, according to the following equation, convert the raw digital numbers (DN) to spectral radiance, L_λ [64],

$$L_\lambda = L_{\min(\lambda)} + \frac{L_{\max(\lambda)} - L_{\min(\lambda)}}{Q_{calmax}} Q_{cal} \quad (1)$$

where L_λ is the spectral radiance, $L_{min(\lambda)}$ = minimum detected spectral radiance for the scene, $L_{max(\lambda)}$ = maximum detected spectral radiance for the scene, Q_{cal} = gray level for the analyzed pixel, and $Q_{cal\ ma}$ = maximum gray level.

The second step was to establish the relationship between the spectral radiance and the radiant temperature for the pixel. The relationship can be described using the following equation:

$$L_\lambda = \frac{K_2}{ln\left(\frac{K_1}{L_\lambda}+1\right)} \quad (2)$$

where K_1 and K_2 are two calibration constants, and Ti = radiant temperature (K). For the TM thermal band 6, K_1 = 607.76 W/(m^2·sr·um) and K_2 = 1260.56 K, and for the ETM+ thermal band 6, K_1 = 666.09 W/(m^2·sr·um) and K_2 = 1282.71 K.

In the final step, we converted the radiant temperature Ti to the surface kinetic temperature T using the following equation,

$$\mathrm{T} = \varepsilon_\lambda^{-1/4} T_i \quad (3)$$

where the ε_λ is the spectral emissivity. According to previous literature, the emissivity values in the spectral region of the TM/ETM+ thermal band range from 0.7 to 1.0 for most natural materials. For sandstone, shale and burnt rocks, the emissivity can be selected as 0.95 [51,52,65,66]. In the paper, the emissivity was estimated at 0.95, which was also used in previous literature in the WCF [67,68].

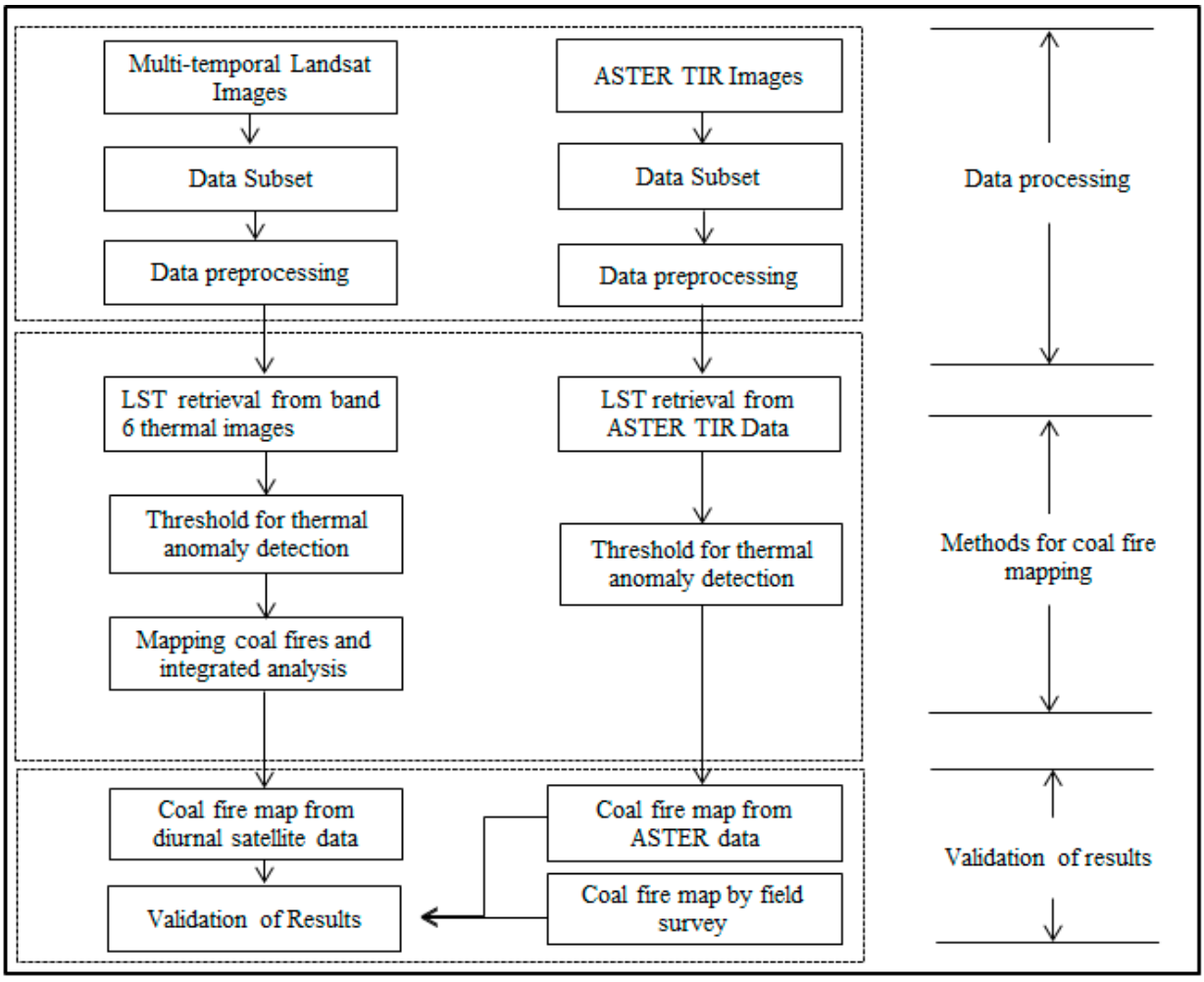

Figure 3. Flow chart for data pre-processing and study analysis.

4.2. LST Retrieval from ASTER TIR Data Using the TES Algorithm

The multi-spectral sensor ASTER onboard the National Aeronautics and Space Administration (NASA) Terra satellite has five channels in the thermal region (8.125–8.475 μm, 8.475–8.825 μm, 8.925–9.275 μm, 10.25–10.95 μm, and 10.95–11.65 μm), which provides an opportunity for scientists to directly estimate emissivity and temperature from the remote sensing data. Recently, researchers have developed several methods for extracting emissivity information from the ASTER imagery, including the TES algorithm, Emissivity Normalization Method (NEM), alpha-derived emissivity method and Reference Channel Method (RCM) [62]. To validate the results that were derived from the multi-temporal Landsat TM/ETM+ thermal band 6 data, we used the temperature products that were derived from the ASTER data using the TES algorithm that was developed by the ASTER research team. The TES algorithm was developed by Gillespie *et al*. [62] to retrieve temperatures (with an accuracy of ±1.5 K) and emissivity (with an accuracy of ±0.015) from the TIR bands of the ASTER imaging radiometer. The TES algorithm combines three algorithms that are linked together, as shown in Figure 4.

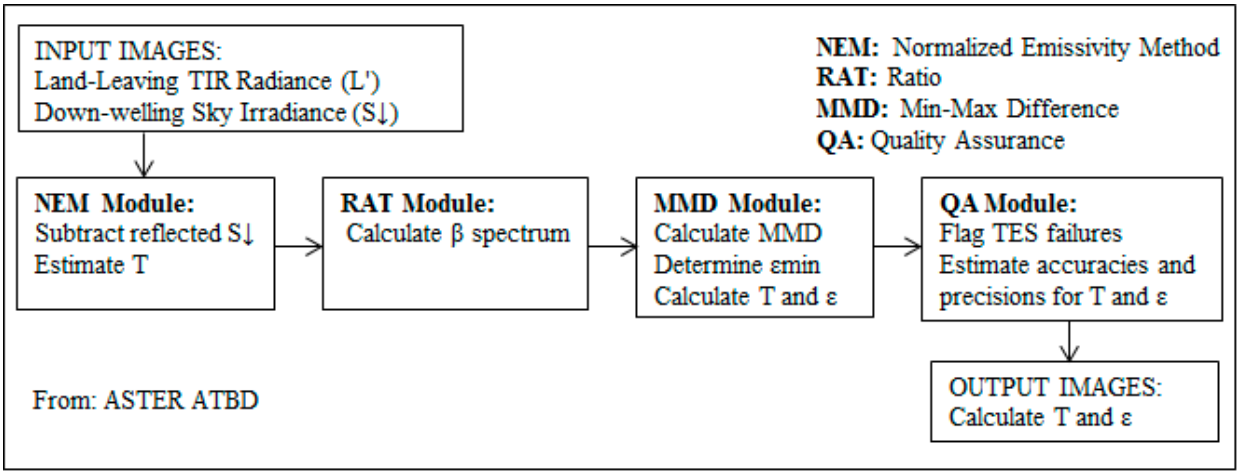

Figure 4. Basic design of the TES algorithm. The NEM module estimates normalized emissivities that are used to estimate the reflected sky irradiance, which is removed iteratively, and then estimates the surface temperature *T*. *T* is used in the RAT module to calculate the normalized emissivities, or β values, which measure the spectral shape. The MMD module calculates the Min-Max β difference, from which the minimum emissivity ε_{min} is found using empirical regression. The β spectrum is scaled by ε_{min} to give the TES emissivities, from which the surface temperature is calculated. Accuracies and precisions are calculated from the data characteristics and measures of TES performance.

TES is an algorithm that was initially developed to retrieve LST and land surface emissivity (LSE) from ASTER images [62]. This algorithm hybridizes three mature modules: NEM, spectral ratio (SR), and min-max difference (MMD).

TES first uses the NEM module to estimate the initial surface temperature and the normalized emissivities from the atmospherically corrected radiances at ground level. The SR module is subsequently used to calculate the ratio of the normalized emissivities to their average:

$$\beta_i = \frac{\varepsilon_i}{\frac{1}{N}\sum_{i=1}^{N}\varepsilon_i} \quad (N \text{ is the total number of TIR channels}) \tag{4}$$

Although the SR β cannot directly provide the actual emissivity, it describes the shape of the emissivity spectra well, even if the surface temperature is roughly estimated. Finally, based on the SR, the MMD module is used to find the spectral contrast in *N* channels:

$$\text{MMD} = max(\beta_i) - \min(\beta_i) \quad (5)$$

To recover the actual values of the emissivities, an empirical relationship between the minimum emissivity (ε_{min}) in the *N* channels and MMD is established:

$$\varepsilon_{min} = 0.994 + 0.687MMD^{0.737} \quad (6)$$

with 0.994, 0.687, and 0.737 as the sensor-dependent coefficients for the ASTER sensor using the laboratory and field emissivity spectra. Once the ε_{min} is estimated, the emissivities in other channels can be straightforwardly derived from the SR β_i using:

$$\varepsilon_i = \beta_i\left(\varepsilon_{min}/min(\beta_i)\right) \quad (\text{i} = 1, \ldots, \text{N}) \quad (7)$$

LST can then be refined and estimated. More details can be found in [52,62].

4.3. Threshold for Coal Fire Delineation Using Landsat TM Band 6 and ASTER TIR Data

Seasonal variations, climatic conditions, types of surface, intensities and depths of the coal fire affected the temperatures retrieved from the multi-temporal thermal images. Therefore, a fixed threshold was not suitable for coal fire delineation, but a dynamic threshold was available for use in this study. A good review of common dynamic threshold setting techniques is presented by Raju *et al.* [69]. For example, the histogram method is one dynamic threshold-setting technique. In this method, the change in the shape of the slope of the histogram is identified, and a hypothetical uniform histogram is projected; the value of the point on the x-axis where this projected slope intersects is used as the threshold. The moving window algorithm is another dynamic threshold setting method for extracting coal fire information. In this method, the histograms are statistically analyzed, and the DN value that represents the first local minimum drop after the primary maximum DN peak is set as the threshold.

Based on the literature pertaining to setting a dynamic threshold and the local climate conditions, we used the automated method in our study. The automated method has commonly been used to discriminate coal fires. This method uses statistical parameters to detect the coal fires under the condition that the satellite data are radiometrically corrected, and the statistical parameters, such as the mean average value of the data $\bar{a}$ and the standard deviation σ, were used to set a threshold. Using this method, $\bar{a} + 2\sigma$ was commonly used to delineate the areas of the coal fires.

However, certain points resulting from the automated method that are based on thermal anomalies in the satellite thermal images may not correspond to true coal fires, e.g., the bulk volume of mining wastes. These mining wastes also have a higher temperature than the background due to opencast mining activities. Therefore, it is of great importance to remove the coal dump from the results of coal fire detection. To address this situation, another factor for a more accurate delineation of coal fires, *i.e.*, spectral reflectance was considered. The type of rock material and the nature of soil depend on the geological characteristics of the underlying rocks. The mining wastes are the rock fragments of associated overlying soil materials and rocks that are piled together in the vicinity of the opencast mining area as an overburden dump. These materials and the overburden dump are commonly sandstone-shale

surfaces, and their chunks and fragments, often with no vegetation. The overburden coal dump and the fresh rock surface provide surfaces of the highest ground reflectance in the area. Subsequently, to remove the coal dump to generate a more accurate delineation of coal fires, it is critical to determine an appropriate threshold to differentiate the coal wastes from the surface areas that are related to cold coal fire (with a temperature less than 150 °C, more details can be found in [68]) using the remotely sensed reflectance data.

The WCF area is mostly an open-cast mine area, and the various ground features are often overburden coal dumps, underground coal fires and some scattered surface coal fires. Among these ground features, the overburden coal dumps had the highest reflectance value. To determine the appropriate threshold to differentiate the coal overburden dumps from the surface areas as related to cold coal fires, the spatial profile analysis method was used for long time series of Landsat TM/ETM+ band 7 reflectance data. Using the FCC map composed of TM/ETM+ 4, 3, 2 and 7, 5, 3 band combinations, several spatial profiles passing through barren exposed materials, coal dumps and underground coal fires were selected. First, the spectral reflectance values along these spatial profiles were analyzed on a pixel-by-pixel basis. Second, the preselected spatial files were traced on all of the images of the temporal stack data. This detailed analysis helped to determine the maximum reflectance value that was associated with overburden coal wastes that are piled together near the coal mining area. Then, the maximum reflectance value was set as the threshold value, and any value of a pixel higher than the threshold was attributed to the overburden coal dumps.

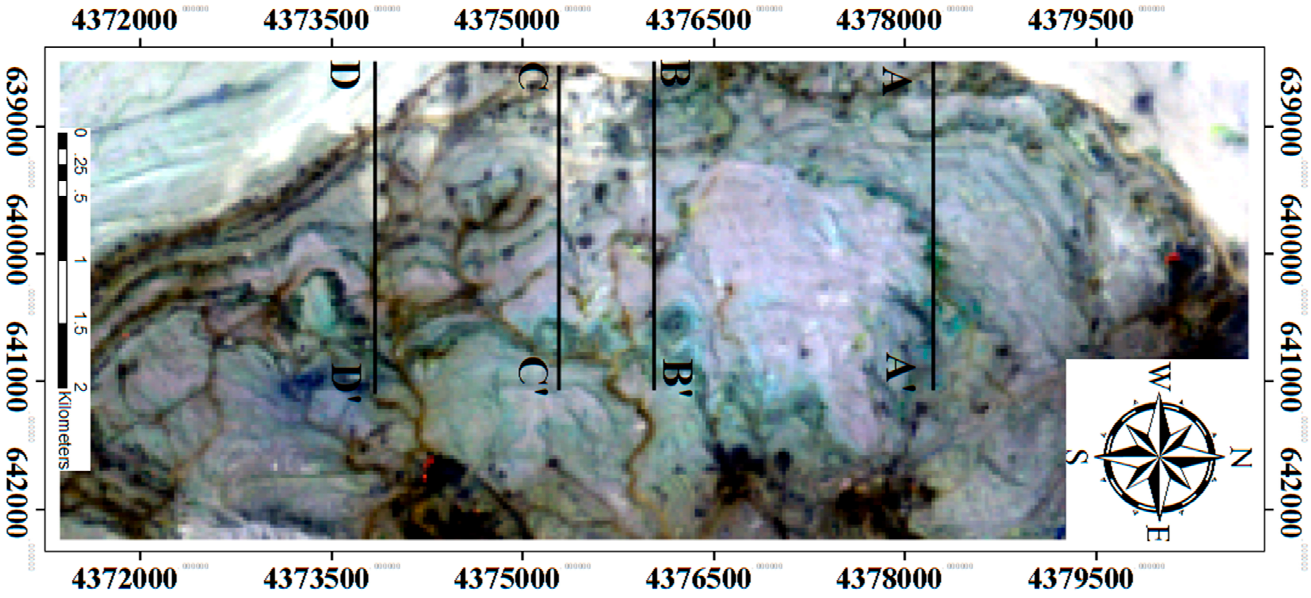

Figure 5. Location of the sampling spatial profiles shown on the 3 May 2003 Landsat TM standard false composite image of WCF.

To determine appropriate threshold to delineate the coal overburden dump to remove these wastes, field survey work was carried out from 6 July 2003 to 15 July 2003 by the Shenhua (Beijing) Remote Sensing (SBRS) Co. Ltd. and the local Wuda Coal Mine Bureau under the co-project under the frame of the Sino-Germany Dragon Program. Selecting the closest-to-the-field-survey-time Landsat TM image, the spatial profiles AA', BB', CC', and DD' were drawn across the 3 May 2003 image (see Figure 5).

For these four profiles (AA', BB', CC', and DD'), the spectral reflectance value along these profiles and the respective maximum reflectance are shown (see Figure 6a–d).

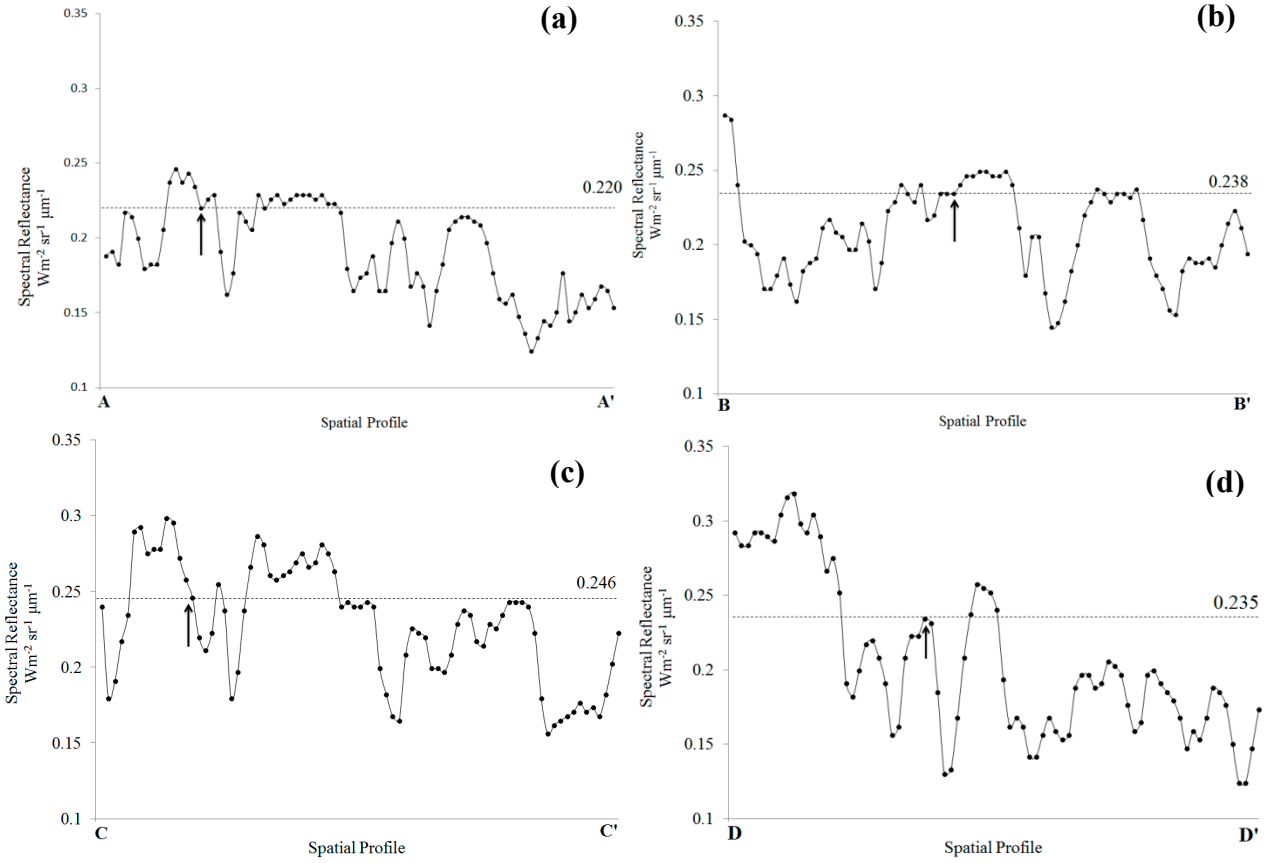

Figure 6. Maximum reflectance along the spatial profiles AA', BB', CC', and DD' that were extracted from the Landsat TM 7 image of 3 May 2003 for WCF. The maximum reflectance of approximately 0.25 (25% reflectance) along the profiles: (**a**) The maximum reflectance along the spatial profile AA'. (**b**) The maximum reflectance along the spatial profile BB'. (**c**) The maximum reflectance along the spatial profile CC'. (**d**) The maximum reflectance along the spatial profile DD'.

The WCF area is mostly an open-cast mine area, and the various ground features are often overburden coal dumps, underground coal fires and some scattered surface coal fires. Among these ground features, the overburden coal dumps had the highest reflectance value (see Figure 7). Therefore, taking the spatial profile DD' as an example (see Figure 7(a)), with the help of the image from 5 Oct. 2003 from Google Earth ™ (see Figure 7(b)) and the field survey photograph (see Figure 7(d) and 7(e)), the pixel corresponding to the overburden coal dumps can be marked and delineated with the determined threshold (see Figure 7(c)). From Figure 6 and Figure 7, a threshold of average reflectance value of 0.24 with the TM7 image corresponded to the overburden coal dumps; therefore, 0.24 was set as the threshold, and the average spectral reflectance value of the pixels of the overburden coal dumps more than 0.24 was undoubtedly due to coal overburden dumps.

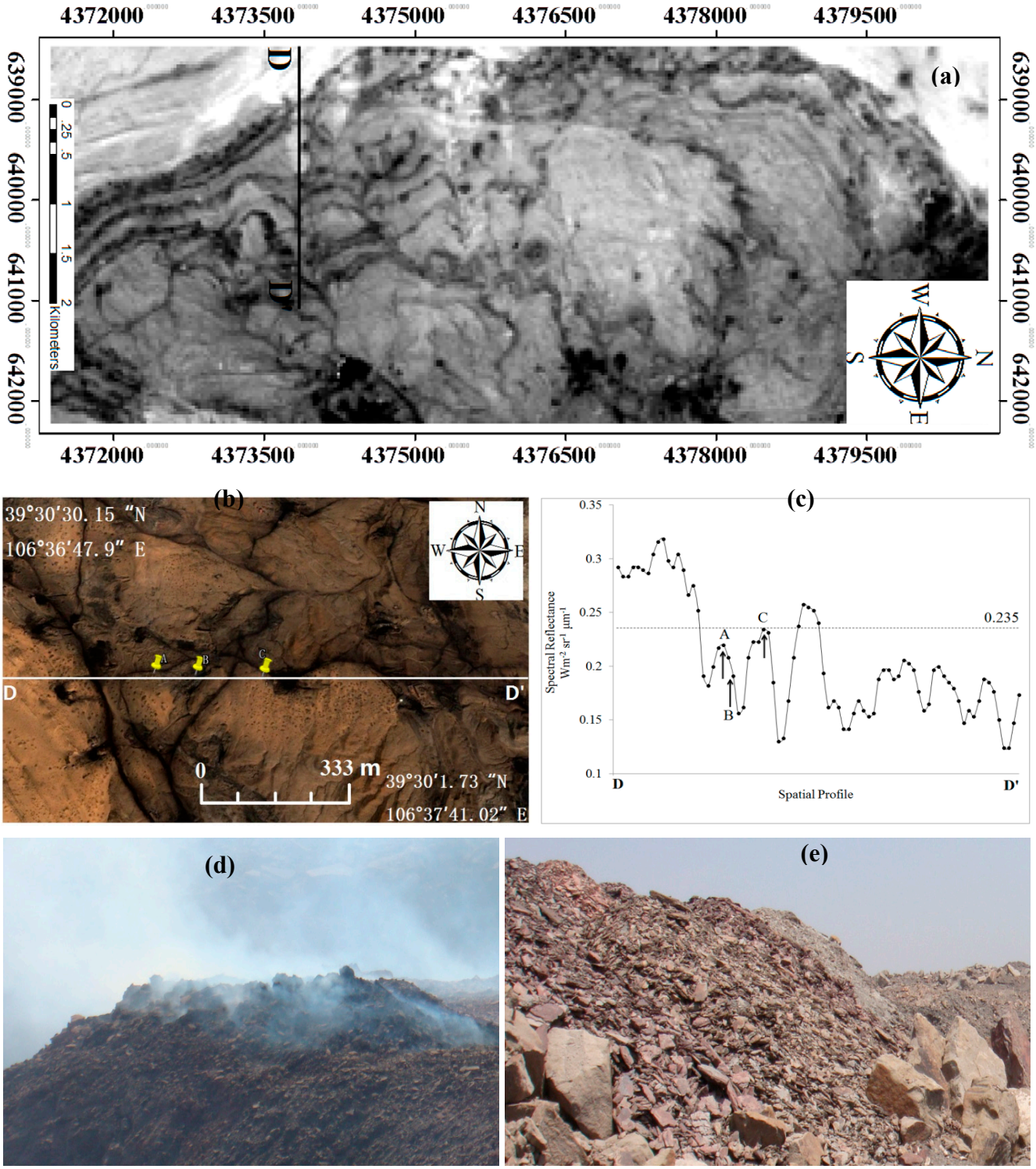

Figure 7. The methodology that was followed in the study to remove coal overburden wastes is presented here with a thresholding method using the WCF as an example. (**a**) The location of the selected profile line DD' on Landsat TM band-7 image of 3 May 2003; (**b**) Underground coal fire location A and B and coal overburden dump location C along the selected spatial profile DD' are shown as a reference on a very high resolution Google Earth TM back ground image of 5 October 2003; (**c**) Maximum reflectance along the spatial profile line DD'; (**d**) Field photograph of a coal fire location B; (**e**) Field photograph of a coal overburden dump at location C.

4.4. Detection of the Spreading Direction of Coal Fire

The coal fire spreading direction can be determined based on the dynamics of coal fires and the spatial distribution of these fires as identified using the multi-temporal TIR remote sensing data. Based on the multi-temporal satellite data, we identified the coal fire spreading direction by stacking the coal fires that were identified in the satellite data from every two successive years using the stacking analysis technique, which analyzes the images in sequence with the help of the Geographic Information System (GIS) software (ArcGIS, ESRI Inc., Redlands, CA, USA). Using specialized GIS software, such as ENVI and IDL, we delineated the coal fires using the automated method. Using the specialized GIS software and the overlay analysis technique, we performed a comparative analysis of the results of every two successive years. Ultimately, we developed a coal-fire spreading-direction map based on the spatial distribution of these temperatures that were extracted from the TM/ETM+ band 6 images.

5. Results and Discussions

5.1. Validation of the Results of Coal Fires

The coal fire map was obtained from the long time series Landsat band 6 data and Terra ASTER data using the threshold setting technique, and this map was validated using the CFM that was produced by the field survey. An attempt was made to perform a cross-validation analysis. Based on the above coal fire information, and using ArcGIS software (Environmental Systems Research Institute, Inc., Red Lands, CA, USA) and the spatial analysis technique, we performed a quantitative analysis of the coal fire dynamics from 1999 to 2006. Subsequently, a comparative analysis of the annual coal fire progression and the prediction of the spreading direction were carried out for the period 1999 to 2006.

5.1.1. Testing of the Continuity of Results That Were Obtained from 2001 ASTER Data and ETM+ Band 6 Data

Because the ASTER data have five thermal bands in the thermal infrared region, ranging from 8.125 μm to 11.65 μm, the LSTs that were derived using the TES algorithm are more accurate than the LSTs that were derived from the Landsat data, which are from a single band in the thermal region from 10.25 μm to 11.45 μm. Therefore, we cross-validated the assessments of the coal fires based on the two types of satellite data. The coal fire assessments were extracted from the two types of satellite data using the same thresholding method based on the statistical parameters (described in Section 4.3), and before the cross-validation, the coal-fire map that was obtained from the 2001 ETM+ data was resampled to the same spatial resolution, 90 m, as the ASTER data.

During the cross-validation, as shown in Figure 8, we found that the coal fire information that was extracted from the 2001 daytime ETM+ data coincides with the coal fire information that was obtained from the ASTER TIR imagery, which showed a good consistency between the two types of results, and that the number of pixels within the intersection region between the two types of results is 90.5 (see Table 2), which accounts for 85.3 percent of total coal fires extracted from the 2001 Landsat data. These findings indicate a good linear relationship between the results of the two procedures.

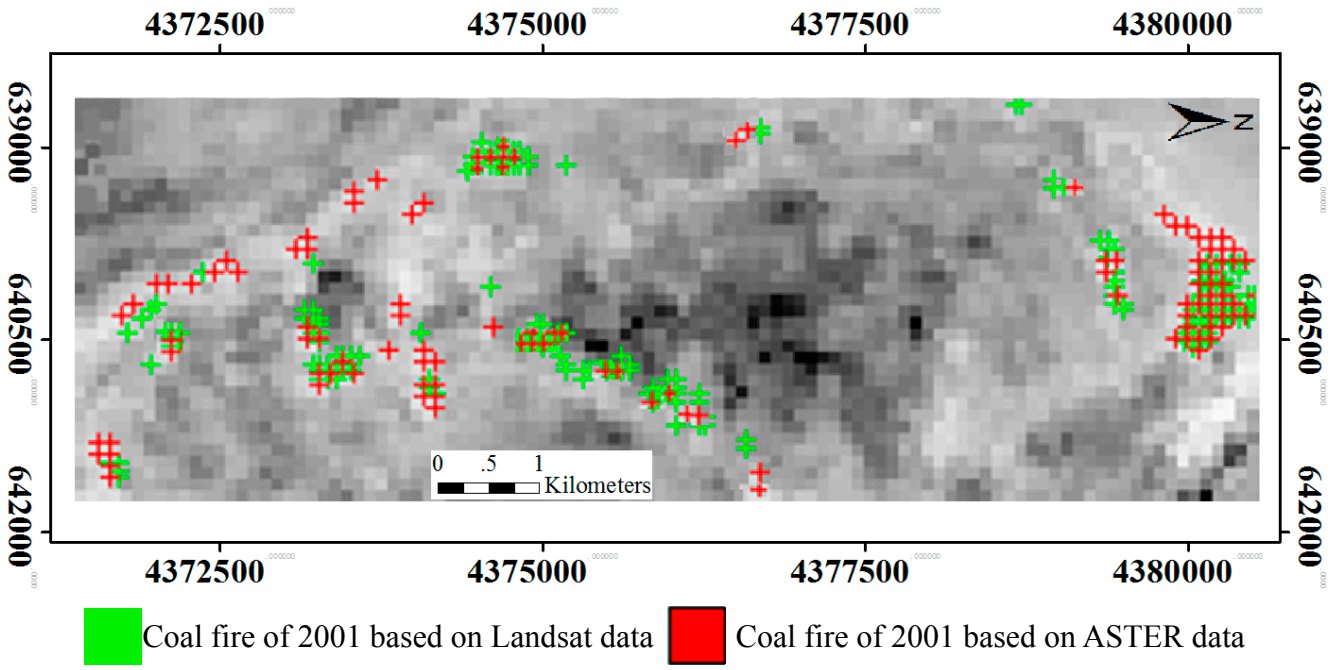

Figure 8. Cross-validation of coal fire information that was extracted from 2001 Landsat and ASTER imageries, the two-year's worth of coal fires were stacked for overlay analysis.

Table 2. Cross-validation of the coal fires from Landsat and ASTER imageries.

Data Type	Acquisition Time	Spatial Resolution	Coal Fires Extracted from Satellite Data	Intersection Part of Coal Fires (%)
ETM+	29 May 2001	90 m	96 Pixels	90.5
ASTER	8 August 2001	90 m	106 Pixels	

5.1.2. Validation of the Results Obtained from 2002 and 2003 ETM+ Band 6 Data Using the Field Survey Map

The field survey map of coal fires was used in the validation of the results from the 2002 and 2003 daytime data. The field survey was carried out in 2002 and 2003, during which time the coal fires were expanding fast and had been burning for nearly 50 years since starting to burn in the 1950s. By 2000, the coal fires had received the attention of the central and local governments, and many scientists were called on to investigate how to control these fires. The local mineral bureau developed a detailed geological survey of the distribution of the coal fires in 2002 and 2003. The resulting coal fire map at a scale of 1:5000 was used to validate our data from the same time period. Before the validation, the coordinates of the fire map were converted to WGS 84, and the spatial resolution was resampled to 60 m, the same as the ETM+ data.

The results from validating the coal fire information of 2002 and 2003 indicated omission errors of 21.5 percent and 26.7 percent, respectively, and commission errors of 3.6 percent and 1.7 percent, respectively (see Table 3). The low commission errors indicated that the results that were obtained from the multi-temporal Landsat data are good for analyzing the coal fire spreading directions. The higher omission error may be explained as follows: based on Figure 9, we found that areas I, II, III, IV and V were the primary sources of omission errors, and the primary reason for coal fires in these areas going

undetected may have been their depth. As is well-known, the deeper the coal fire is, the less heat is conducted to the surface. Consequently, temperature differences are less conspicuous, leading to more difficulty in discriminating coal files using the remote sensing technique. Another reason for the omission error may be that the spatial resolution of the Landsat data is lower, with a pixel size of 60 m × 60 m, whereas certain coal fires may be so small that they cannot be detected. Areas VI, VII and VIII are the primary sources of commission errors. The primary reason for mistaking these areas for coal fires may be the influence of solar radiation on the surface temperatures. Another reason may be the time lapse effects. The coal fires expanded at an average rate of 5 m per month. Certain points may have been true coal fires that appeared in the 2002 results but were burnt out before the CFM was finished, whereas other points may have appeared as coal fires in the 2003 results but began to burn after the coal fire survey was completed.

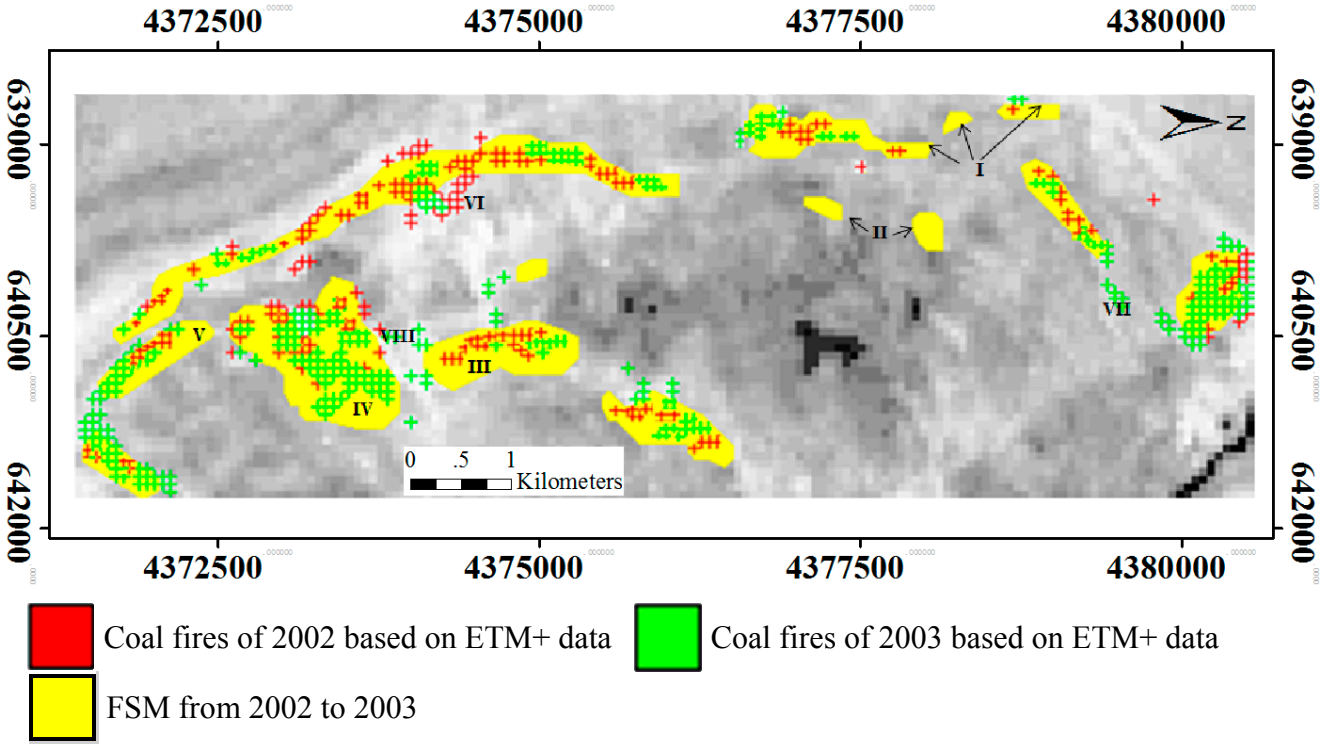

Figure 9. Validation of the coal fire information that was extracted from 2002 and 2003 Landsat data using the coal fire map by the field survey from 2002 to 2003, with the three-year results of coal fires stacked for the overlay analysis.

Table 3. Validating the results of the coal fires based on 2002 and 2003 Landsat data using the coal fire map from the field survey. FSM: Field Survey Map.

Data Type	Acquisition Time	Spatial Resolution	Omission Error (%)	Commission Error (%)
ETM+	20 August 2002	60 m	21.5	3.6
FSM	2002–2003	60 m		
ETM+	3 May 2003	60 m	26.7	1.7
FSM	2002–2003	60 m		

5.2. Analysis of the Coal Fire Spreading Direction from 1999 to 2006

Using the automated method on the basis of statistical parameters, the areas of the coal fires were extracted from the multi-temporal Landsat TM/ETM+ data from 1999 to 2006 (see Table 4). However, it seemed complex and impractical to combine all of the satellite data when performing an overlay analysis. Therefore, the coal fires that were extracted from every two adjoining years of data were overlaid to investigate the dynamics of the coal fires (see Figures 10–13). To conveniently display the coal fire spreading direction, the areas of the coal fire belts were divided into three regions: A, B and C.

Table 4. Threshold for coal fire mapping and the corresponding area based on satellite data.

Data Type	Spatial Resolution (m)	Acquisition Time	Threshold (K)	Area of Coal Fire (m^2)
ETM+	120	12 August 1999	316.0	309,600
ETM+	120	30 August 2000	313.0	651,600
ETM+	120	29 May 2001	316.0	684,000
ETM+	120	20 August 2002	308.0	770,400
ETM+	120	3 May 2003	315.0	838,800
TM	120	17 August. 2004	308.0	918,800
TM	120	7 August 2006	310.0	1,015,400

The coal fires that were extracted from the 1999 and 2000 Landsat data were overlaid to perform a comparative analysis, as shown in Figure 10. In Figure 10, it is clear that fire zones II-1, II-2, II-3 and II-4 are in the dotted-line-rectangle B. Most of the coal fires in this area spread north or northeast, whereas in the northernmost part of the WCF, region C, the coal fires in zone III-1 were inclined to spread southwest. In the southernmost part of the WCF, area A, some coal fires, such as I-1 and I-2, were inclined to spread southwest, except for certain points of fire scattered around them. There were additional coal fires that were inclined to spread laterally away from a zone of origin to some extent. The central line was regarded as an original coal fire belt that had a higher temperature than that of its two sides, which caused the coal fires to spread laterally away from the central line.

The coal fires that were extracted from the 2000 and 2001 Landsat data were overlaid to perform a comparative analysis, as is shown in Figure 11. In Figure 11, as was described above, we used a dotted-line-rectangle B to describe the middle region of the WCF. In region B, we found that coal fire zones V-1 and V-2 tended to spread northwest, whereas the coal fire zones V-3 and V-4 had a tendency to spread northeast. In the southern end of the WCF, coal fire zone IV in region A had a tendency to expand northwest. In the northern part of the WCF, the double arrow of coal fire zone VI-2 in region A was spreading southeast, whereas coal fire zone VI-1 was expanding laterally away from a central line.

The coal fires that were extracted from the 2002 and 2003 Landsat data were overlaid to perform a comparative analysis, as is shown in Figure 12. In this Figure, in region B, it was clear that most of the coal fires were expanding outward in three directions: north, northeast and northwest. These fires were developing very fast during the period from 2002 to 2003, and the coal fire zones VIII-1, VIII-2, VIII-3, VIII-4 and VIII-5 in the middle region B are good examples for interpretations. Based on this figure, we can see that in coal fire zone VII in region C, in the southern part of the study area, the double arrow for this fire zone shows the spreading direction of coal fires toward both sides, from the middle southwest and northeast. In the northern end of the WCF in region C, the double arrow of coal fire zone IX also had a tendency to expand

outward in the opposite directions: southeast and northwest.

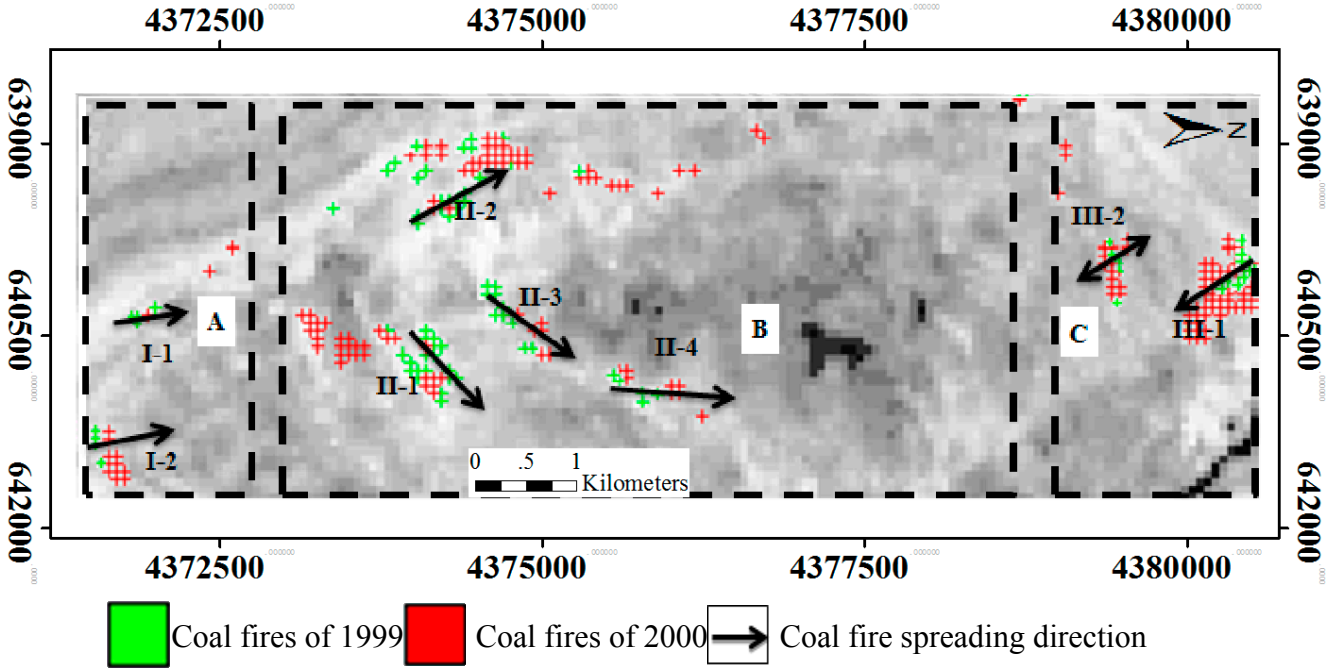

Figure 10. Coal fire map from 1999 to 2000. The results of the coal fires of 1999 and 2000 were stacked for the overlay analysis, and the coal fire spreading directions were also delineated as shown in this image with the 1999 ETM+ TIR band 6 data as the base map. According to the spatial distribution of the coal fires, we divided the entire study area into three main regions of coal fires.

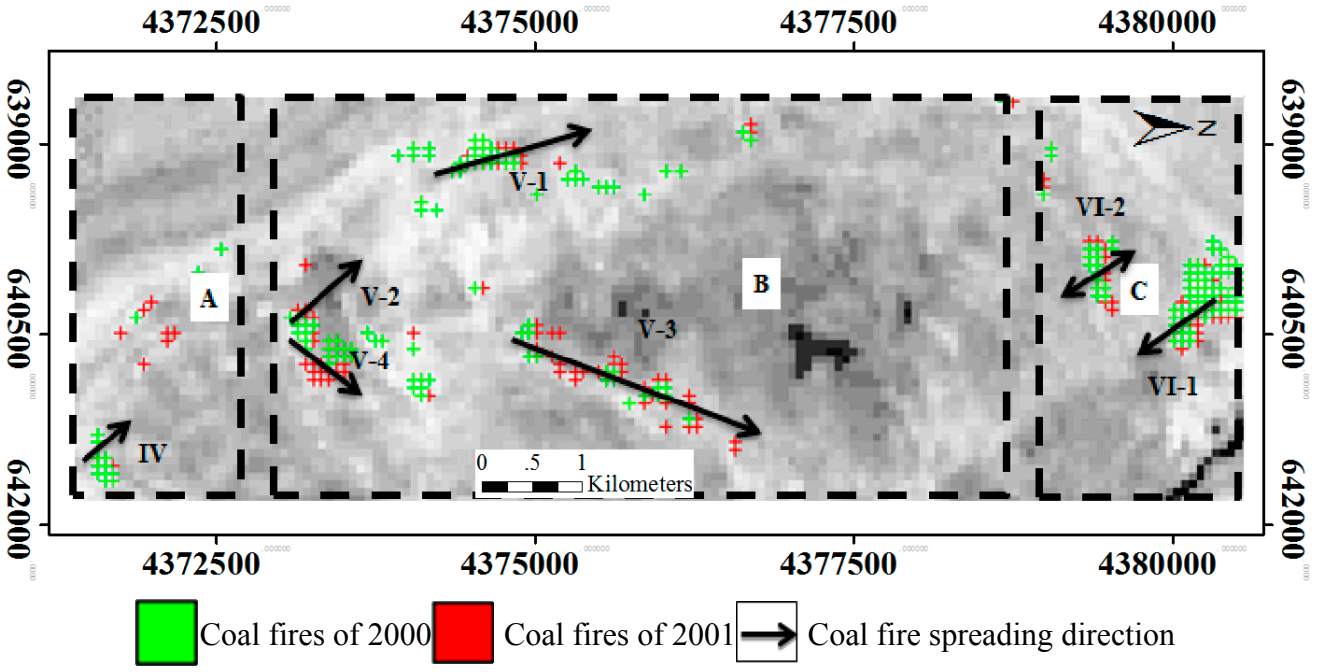

Figure 11. Coal fire map from 2000 to 2001. The results of the coal fires of 2000 and 2001 were stacked for the overlay analysis, and the coal fire spreading directions were also delineated as shown in this image.

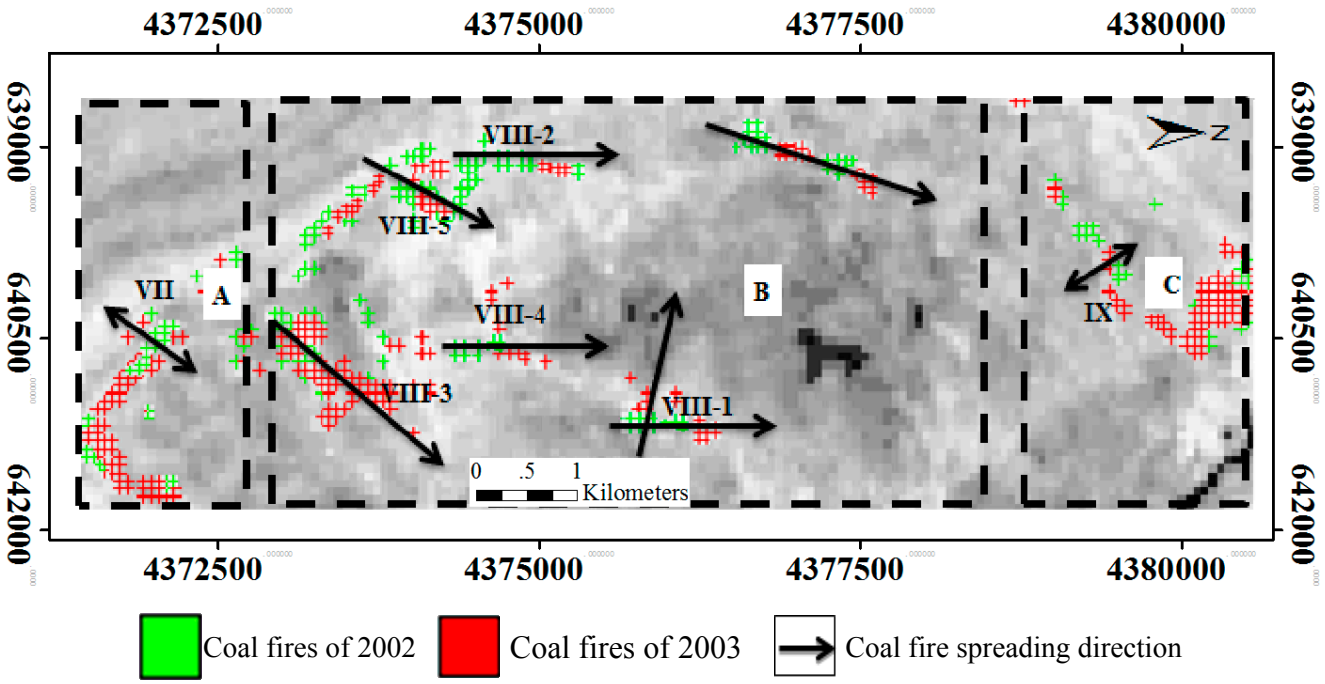

Figure 12. Coal fire map from 2002 to 2003. The results of the coal fires of 2002 and 2003 were stacked for the overlay analysis, and the coal fire spreading directions were also delineated as shown in this image.

The coal fires that were extracted from the 2004 and 2006 Landsat data were overlaid to perform a comparative analysis, as is shown in Figure 13. In this figure, coal fire zone XI-1 in area B was spreading approximately northeast, whereas the coal fire zones XI-2, XI-3 and XI-4 were believed to have a tendency to spread north. In the northern end of the study area, coal fire zone XII-1 was spreading south or southwest, and the double arrow of coal fire zone XII-2 shows the spreading direction of coal fires toward to both sides from the middle. When this coal fire burnt out after 2004, the fire was then believed to tend to spread east. In the southern end of the WCF, coal fire zone X-1 was predicted to spread outward in opposite directions: southwest and northeast. When this coal fire burnt out after 2004, the fire began to spread northwest. Within this same area, coal fire zone X-2 was also believed to expand northwest.

To perform an accurate and convenient comparative analysis and to develop clear conclusions regarding the coal fire dynamics that were obtained from long time series satellite data from 1999 to 2006, the results of 2000, 2002, 2004 and 2006 were chosen, using the 1999 Landsat TIR data as the base map to depict the spread of coal fires during that period (see Figure 14). It is important and conspicuous that there are 6 primary coal-fire-related thermal anomalies with linear shapes, which we called thermal anomaly belts. Considering the intensity and the degree of consistency of coal fire distribution (which can be seen by the results of coal fires that were obtained from the Landsat data), these coal fire belts were divided into three regions: A, B and C. Coal-fire-related thermal anomaly belt I was located in region A. Another four primary coal fire thermal anomaly belts (II, III, IV and V) were located in region B, and the thermal anomaly belts VI, VII and VIII were located in region C (see Figure 15). The spreading direction of thermal anomaly belt I gradually evolved and developed from the original spotty distribution of thermal anomalies. It is clear that the coal fire that was related to this thermal anomaly belt had a spotty distribution in 2000 or 2002, until 2004 and particularly 2006, after

which it assumed a bilateral spreading direction and expanded to form a band with a definite width. After 2006, thermal anomaly belt I was inclined to spread north. Belt II was spreading northeast based on the 2000 to 2006 results. Comparing the 2000 and 2002 data, we found that belt III was spreading northeast and that belt IV was inclined to extend northwest or northeast due to its various parts. Belts VI, VII and VIII were spreading southwest, southwest and bilaterally away from the belt, respectively, which can be seen from the analysis of the 2000–2006 data. Generally speaking, we found that the coal fires in the central part of the study area in the WCF were spreading north, northeast, and northwest and that the coal fires in the northern and southern ends of the study area were spreading bilaterally in opposite directions, except for certain coal fires in region A, which tended to spread north or northwest, and certain coal fires in region C, which tended to spread southwest. The results were also validated by later work of other scientists. The No. 18 (designations for coal fires were assigned by the Local Mineral Bureau) coal fire area, which was located in the central southern district along the boundary between the Suhaitu mine and Huangbaici mine (latitude 39°31′22″N to 39°31′30″N and longitude 106°38′00″E to 106°38′12″E), is a good example of this type of research. The coal fires in the WCF were also studied by Kong *et al.* [70], with funding from a Sino-German cooperative project. Kong found that the northern part of the No. 18 coal fire in Wuda coal field was spreading north, the eastern part was spreading north, and the eastern and southern parts were extended to the north along the coal seams. The overall trend of coal fire development was to the north and east, and the velocity of spreading was 3 to 5 m per month [70], which is highly consistent with the results of coal fire spreading direction that were generated in the paper.

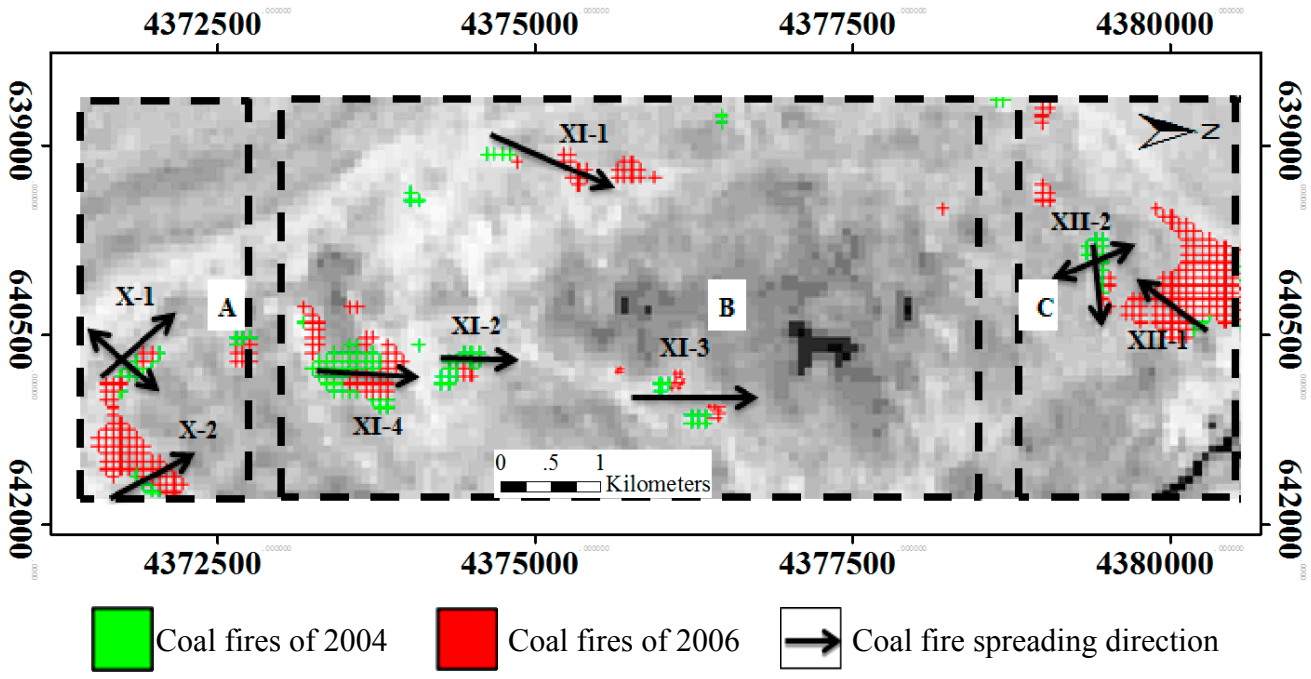

Figure 13. Coal fire map from 2004 to 2006. The results of the coal fires of 2004 and 2006 were stacked for the overlay analysis, and the coal fire spreading directions were also delineated as shown in this image.

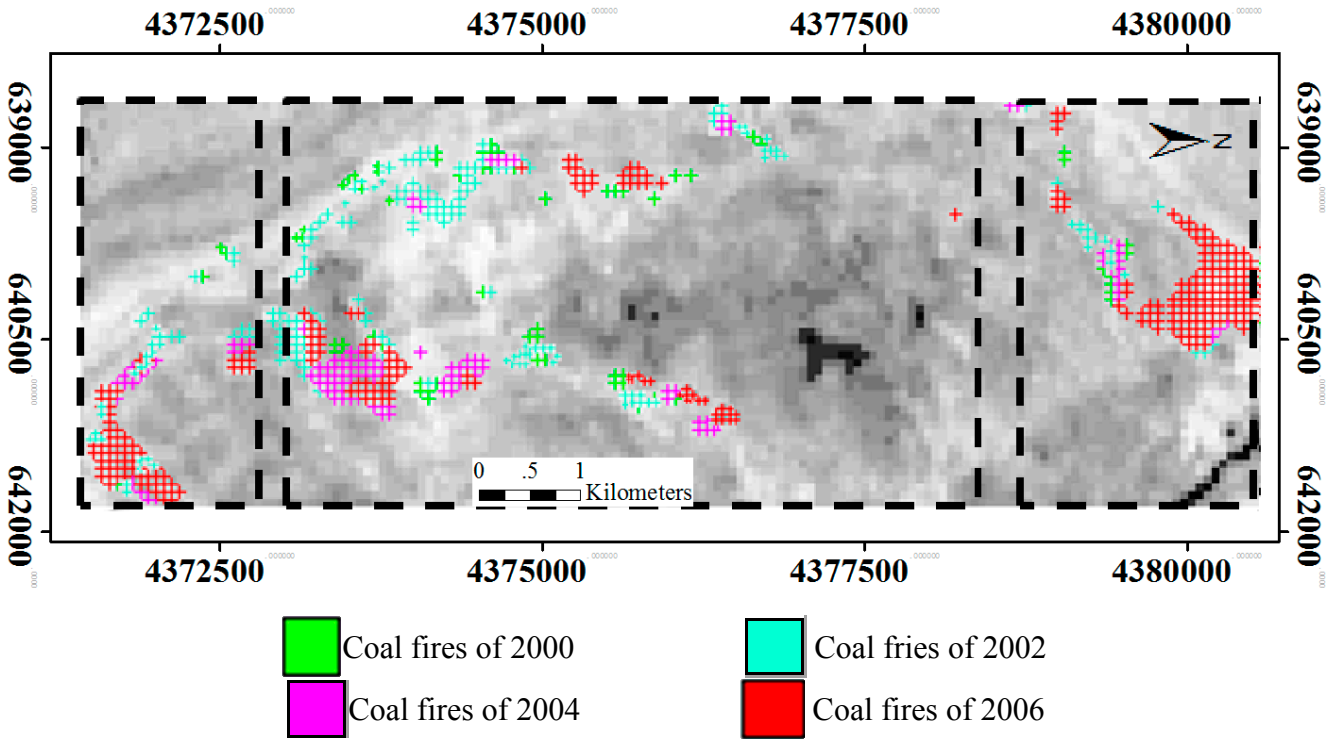

Figure 14. Four years' worth of coal fires results were chosen from the time range 2000–2006. To show the coal fire spreading direction directly and simply using the GIS software ArcGIS and ENVI, the results of coal fires of 2000, 2002, 2004 and 2006 were stacked for the purpose of the overlay analysis, and the coal fire spreading directions were also delineated in this image with the 1999 ETM+ TIR band 6 data as the base map.

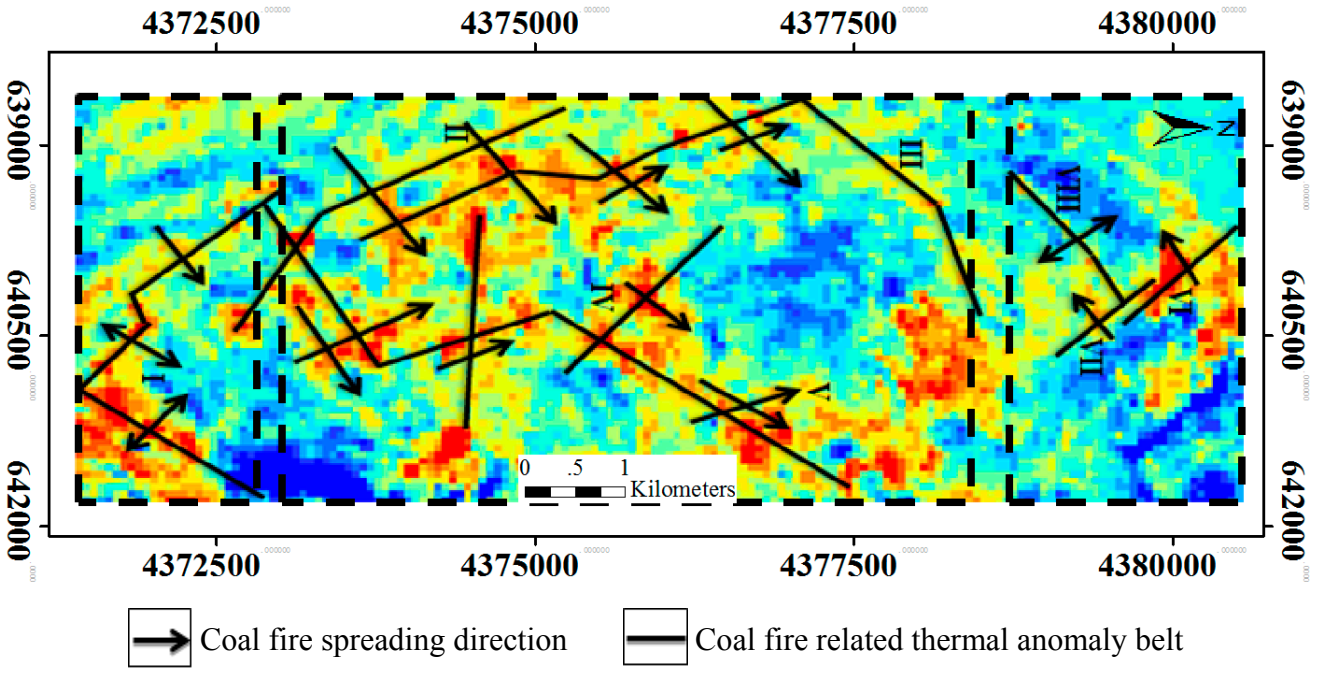

Figure 15. Coal fire spreading direction predicted based on the coal fires that were extracted from long-time series satellite data (See Figure 11) and the base map was 1999 Landsat ETM+ thermal band 6 data, which was sliced with the color table using the ENVI software. The lines of the coal fire spreading direction were drawn using ArcGIS software.

6. Conclusions

In general, the coal fire dynamics analysis addressed the following two aspects: first, the areas of change in spatial extent that were affected by the coal fires and second, the propagation of coal fires that developed from 1999 to 2006. A marked increase in the spatial extent of coal-fire-affected areas from 1999 to 2006 was observed in this research. The coal fires have spatially increased by nearly 0.75 km^2 from 1999 to 2006, with an average annual increase of approximately 0.101 km^2. The spreading direction of coal fires was determined based on the coal fires that were extracted from long time series of satellite data. The results showed that the coal fires in the central part of the study area in the WCF were spreading in three directions: north, northeast and northwest. The coal fires on the northern end of the study area underwent net bilateral propagation, spreading bilaterally in opposite directions: south-north or southwest-northeast. The coal fires on the southern end of the study area underwent net bilateral propagation, spreading bilaterally and also in opposite directions: southeast-northwest, and some certain coal fires in the northern region of the study area underwent net lateral propagation with the intent of spreading toward the southwest.

This study of the direction of coal fire spreading based on TIR remote sensing may be considered important as an attempt to investigate the direction of coal fire spreading on the scale of an entire coal field. The results showed that the TIR remote sensing is an available technique for detecting and mapping coal fires and their spreading direction, particularly in unexplored areas. The non-fixed thresholding method is useful and adequate for quantitative coal fire analysis. A geologic map showing the coal distribution is very important in investigating the direction of coal fire spreading. However, the climatic conditions that vary with the date of acquisition of the satellite data and the variations in environmental and terrain factors may have various effects on the data retrieved from satellites. Furthermore, the SWIR TM7 is proved to be useful to remove the impacts of overburden coal dumps on the results of coal fires, and the threshold of average reflectance value 0.24 appears to work well to delineate the overburden coal dumps. In addition, further research is required as some problems and difficulties have not been resolved in the paper. For instance, considering the limited spatial extent of the surface and subsurface coal fires, with a lower and coarser spatial resolution of Landsat TM/ETM+ thermal data, it is difficult to definitely delineate the surface coal fires from the subsurface coal fires because the surface coal fires pixel-aggregated temperature did not always attain the saturation temperature of the Landsat thermal channel (which is approximately 70 °C). We believe that the multi-temporal nocturnal satellite/airborne thermal data with higher spatial resolution may be more useful and yield more accurate results than daytime data because nocturnal data are unaffected by solar radiation and the topographic effects on thermal radiation may be negligible. In addition, the contrast between a thermal anomaly and the background is relatively high and conspicuous, which is helpful in coal fire information extraction. The coal fire spreading directions from 1999 to 2006 that were observed and imaged based on the multi-temporal satellite datasets were also determined by other environment and climate factors, such as the direction and speed of wind and the incidence of rain. Therefore, with the knowledge of the local environment, climate conditions and geological and geomorphological and terrain data, it is very helpful for us to understand the nature and principle of coal fire dynamics and the corresponding propagation.

Acknowledgements

This work was supported by the Strategic Pilot Scientific & Technological Project of CAS (XDA05030200), by a grant from the National Science and Technology Major Project (2011ZX05039-004), by a grant from the National Key Basic Research Program (973 Program, 2013CB733402), by a grant from the National High Technology Research and Development Program of China (863 Plan, 2012AA121103), by a grant from the National Natural Science Foundation of China (41231170), by a grant from the Ph.D. Programs Foundation of Tianjin Normal University (52XB1108), by a grant from the National Natural Science Foundation of China (41201375), by a grant from the Tianjin Research Program of Application Foundation and Advanced Technology (14JCQNJC07900), by the Tianjin Science and Technology Planning Project (14ZCZDSF00019) and by the Tianjin Science and Technology Planning Project (14TXGCCX00015). The Landsat datasets that were used in this study were all obtained from the U.S. Geological Survey (USGS) website.

Author Contributions

The authors contributed equally to this work. Xiaoguang Jiang, Xianfeng Song, and Tiejun Cui supervised this paper. Ping Zhou and Caixia Gao provided valuable advice during the process of satellite imaging. Enyu Zhao, Yuze Zhang, and Yi Lian did much of the work of data preprocessing. Shiyue Zhang, Huili Zhang, and Zhuoya Ni carried out the specific process of temperature retrieval. Hongyuan Huo wrote the paper.

Conflicts of Interest

The authors declare no conflict of interest.

References

1. Gangopadhyay, P. Coalfire Detection and Monitoring in Wuda, North China: A Multi-Spectral and Multi-Sensor TIR Approach. Master's Thesis, International Institute for Geo-Information Science and Earth Observation (ITC), Enschede, The Netherlands, 2003.
2. Banerjee, S.C. *Spontaneous Combustion of Coal and Mine Fires*; A. A. Balkema: Rotterdam, The Netherlands, 1985.
3. Schmal, D.; Duyzer, J.H.; van Heuven, J.W. A model for the spontaneous heating of coal. *Fuel* **1985**, *64*, 963–972.
4. Fisher, W.J.; Knuth, W.M. Detection and delineation of subsurface coal fires by aerial infrared scanning. *Geol. Soc. Am. Spec. Pap.* **1968**, *115*, 67–68.
5. Greene, G.W.; Moxham, R.M. Aerial Infrared surveys and borehole temperature measurements of coal mine fires in Pennsylvania. In Proceeding of the 6th Symposium on Remote Sensing of Envrionment, Ann Arbor, MI, USA, 13–16 October 1969; pp. 517–525.
6. Ellyett, C.D.; Fleming, A.W. Thermal infrared imagery of the burning mountain coal fire. *Remote Sens. Environ.* **1974**, *3*, 79–86.
7. Sinha, P.R. Mine fires in Indian coalfields. *Energy* **1986**, *11*, 1147–1154.

8. Mukherjee, T.K.; Bandyopadhyay, T.; Pande, S. Detection and delineation of depth of subsurface coalmine fires based on an airborne multispectral scanner survey in a part of the Jharia coalfield, India. *Photogramm. Eng. Remote Sens.* **1991**, *57*, 1203–1207.
9. Cassells, C.; van Genderen, J.; Zhang, X. Detection and measuring underground coal fires by remote sensing. In Proceddings of 8th Australia Remote Sensing Conference, Canberra, ACT, Austrilia, 25–29 March 1996; pp. 90–101.
10. Stracher, G.B. Coal fires: A burning global recipe for catastrophe. *Geotimes* **2002**, *47*, 36–37.
11. Finkelman, R.B. Potential health impacts of burning coal beds and waste banks. *Int. J. Coal Geol.* **2004**, *59*, 19–24.
12. Whitehouse, A.E.; Mulyana, A.A.S. Coal fires in Indonesia. *Int. J. Coal Geo.* **2004**, *59*, 91–97.
13. Agarwal, R.; Singh, D.; Chauhan, D.; Singh, K. Detection of coal mine fires in the Jharia coal field using NOAA/AVHRR data. *J. Geo. Eng.* **2006**, *3*, 212–218.
14. Kuenzer, C.; Zhang, J.; Tetzlaff, A.; van Dijk, P.; Voigt, S.; Mehl, H.; Wagner, W. Uncontrolled coal fires and their environmental impacts: Investigating two arid mining regions in north-central China. *Appl. Geogr.* **2007**, *27*, 42–62.
15. Zhou, L.; Zhang, D.; Wang, J.; Huang, Z.; Pan, D. Mapping land subsidence related to underground coal fires in the Wuda coalfield (northern China) using a small stack of ALOS PALSAR differential interferograms. *Remote Sens.* **2013**, *5*, 1152–1176.
16. Huo, H.; Jiang, X.; Song, X.; Li, Z.-L.; Ni, Z.; Gao, C. Detection of coal fire dynamics and propagation direction from multi-temporal nighttime Landsat SWIR and TIR data: A case study on the Rujigou coalfield, Northwest (NW) China. *Remote Sens.* **2014**, *6*, 1234–1259.
17. Huo, H.; Jiang, X.; Song, X.; Ni, Z.; Gao, C.; Zhang, Y.; Liu, L. A study on spreading direction of coal-fire based with TIR remote sensing in Wuda Coalfield from 2000 to 2006, Northern China. *IOP Conf. Ser.: Earth Environ. Sci*. **2014**, *17*, doi:10.1088/1755-1315/17/1/012087.
18. Kuenzer, C.; Strunz, G.; Voigt, S.; Wagner, W. Multitemporal landcover investigations in an arid mining environment: Coal fire areas in northern China. In Proceeding of the Conference of the EARSel Special Interest Group on Land Use and Land Cover, Dubrovnik, Croatia, 25–27 May 2004; pp. 125–134.
19. Kuenzer, C.; Voigt, S.; Morth, D. Investigating land cover changes in two Chinese coal mining environment using partial unmixing. In Proceedings of the GGRS Conference 2004, Applications in Geosciences, Gottinger, Germany, 7–8 October 2004; pp. 31–37.
20. Chen, Y.; Jing, L.; Bo, Y.; Shi, P.; Zhang, S. Detection of coal fire location and change based on multi-temporal thermal remotely sensed data and field measurements. *Int. J. Remote Sens.* **2007**, *28*, 3173–3179.
21. Kuenzer, C.; Hecker, C.; Zhang, J.; Wessling, S.; Wagner, W. The potential of multidiurnal MODIS thermal band data for coal fire detection. *Int. J. Remote Sens.* **2007**, *29*, 923–944.
22. Kuenzer, C.; Wessling, S.; Zhang, J.; Litschke, T.; Schmidt, M.; Schulz, J.; Gielisch, H.; Wagner, W. Concepts for green house gas emission estimation of underground coal seam fires. *Geophys. Res. Abstr.* **2007**, *9*, 11716.
23. Kuenzer, C.; Zhang, J.; Li, J.; Voigt, S.; Mehl, H.; Wagner, W. Detecting unknown coal fires: Synergy of automated coal fire risk area delineation and improved thermal anomaly extraction. *Int. J. Remote Sens.* **2007**, *28*, 4561–4585.

24. Song, Z.; Kuenzer, C. Coal fires in China over the last decade: A comprehensive review. *Int. J. Coal Geol.* **2014**, *133*, 72–99.
25. Peng, F.; Li, J.J. Aplication of the ground radon exploration on the coal spontaneous resource. *West-China Explor. Eng.* **2007**, *12*, 98–100. (In Chinese)
26. Zhang, J.; Kuenzer, C.; Tetzlaff, A.; Oertel, D.; Zhukov, B.; Wagner, W. Thermal characteristics of coal fires 2: Results of measurements on simulated coal fires. *J. Appl. Geophys.* **2007**, *63*, 135–147.
27. Li, A. Application of radon measure technique for fire exploration extinguishing in ventilating shaft of Dongshan coal mine. *Coal Technol.* **2008**, *27*, 65–67. (In Chinese)
28. Gangopadhyay, P.K. Coalfires Related CO_2 Emissions and Remote Sensing. Ph.D. Thesis. International Institute for Geo-Information Science and Earth Observation (ITC), Enschede, The Netherlands, 2008.
29. Meng, X.; Chu, R.; Wu, G.; Xu, H.; Zhu, J.; Wang, Z. Thermogravimetric study of the effect of a PVA oxygen-insulating barrier on the spontaneous combustion of coal. *Min. Sci. Technol. (China)* **2010**, *20*, 882–885.
30. Abbott, W.E. *Mount Wingen and the Wingen Coal Measures*; Angus & Robertson: Sydeny, NSW, Austrilia, 1918.
31. Davis, S.M.; Landgrebe, D.A.; Phillips, T.L.; Swain, P.H.; Hoffer, R.M.; Lindenlaub, J.C.; Silva, L.F. *Remote Sensing: The Quantitative Approach.* McGraw-Hill Int. Book Co.: New York, NY, USA, 1978.
32. Chuvieco, E.; Congalton, R.G. Application of remote sensing and geographic information systems to forest fire hazard mapping. *Remote Sens. Environ.* **1989**, *29*, 147–159.
33. Ram, B.; Kolarkar, A. Remote sensing application in monitoring land-use changes in arid Rajasthan. *Int. J. Remote Sens.* **1993**, *14*, 3191–3200.
34. Rosema, A.; van Genderen, J.; Schalke, H. *Environmental Monitoring of Coal Fires in North China*; Project Identification Mission Report; Delft Beleids Commmissie Remote Sensing (BCRS): Delft, The Netherlands, 1993; Volume 93, p. 29.
35. Sobrino, J.; Raissouni, N. Toward remote sensing methods for land cover dynamic monitoring: Application to Morocco. *Int. J. Remote Sens.* **2000**, *21*, 353–366.
36. Melesse, A.M.; Weng, Q.; Thenkabail, P.S.; Senay, G.B. Remote sensing sensors and applications in environmental resources mapping and modelling. *Sensors* **2007**, *7*, 3209–3241.
37. Duan, S.-B.; Li, Z.-L.; Tang, B.-H.; Wu, H.; Tang, R.; Bi, Y.; Zhou, G. Estimation of diurnal cycle of land surface temperature at high temporal and spatial resolution from clear-sky MODIS data. *Remote Sens.* **2014**, *6*, 3247–3262.
38. Huo, H.; Ni, Z.; Jiang, X.; Zhou, P.; Liu, L. Mineral mapping and ore prospecting with HyMap data over eastern Tien Shan, Xinjiang Uyghur Autonomous Region. *Remote Sens.* **2014**, *6*, 11829–11851.
39. Lu, J.; Tang, R.; Tang, H.; Li, Z.-L.; Zhou, G.; Shao, K.; Bi, Y.; Labed, J. Daily evaporative fraction parameterization scheme driven by day-night differences in surface parameters: Improvement and validation. *Remote Sens.* **2014**, *6*, 4369–4390.
40. Zhang, D.; Tang, R.; Zhao, W.; Tang, B.; Wu, H.; Shao, K.; Li, Z.-L. Surface soil water content estimation from thermal remote sensing based on the temporal variation of land surface temperature. *Remote Sens.* **2014**, *6*, 3170–3187.

41. Zhao, W.; Li, A.; Bian, J.; Jin, H.; Zhang, Z. A Synergetic algorithm for mid-morning land surface soil and vegetation temperatures estimation using MSG-SEVIRI products and TERRA-MODIS products. *Remote Sens.* **2014**, *6*, 2213–2238.
42. Slavecki, R.J. Detection and location of subsurface coal fires. In Proceedings of the Third Symposium on Remote Sensing of Environment, Ann Arbor, MI, USA, 14–16 October 1964; pp. 537–547.
43. Künzer, C.; Zhang, J.; Voigt, S.; Center, G.R.S.D. Set up of a spectral database for unmixing approaches in mining environments in north-central China: Demarcating coal fire risk areas. In Proceedings of the 3rd EARSeL Workshop on Imaging Spectroscopy, Starnberg, Germany, 13–16 May 2003; pp. 344–348.
44. Zhang, X.; Zhang, J.; Kuenzer, C.; Voigt, S.; Wagner, W. Capability evaluation of 3–5 μm and 8–12.5 μm airborne thermal data for underground coal fire detection. *Int. J. Remote Sens.* **2004**, *25*, 2245–2258.
45. Gangopadhyay, K.P.; Lahiri-Dutt, Kuntala. *Detecting Coalfires with Remote Sensing: A Comparative Study of Selected Countries*; Resource Management in Asia-Pacific Working Paper No. 58; Resource Management in Aisa-Pacific Program, Research School of Pacific and Aisan Studies, The Australian National University: Canberra, ACT, Australia, 2005.
46. Gangopadhyay, P.K.; Maathuis, B.; van Dijk, P. ASTER-derived emissivity and coal-fire related surface temperature anomaly: A case study in Wuda, North China. *Int. J. Remote Sens.* **2005**, *26*, 5555–5571.
47. Künzer, C. Demarcating Coal Fire Risk Areas Based on Spectral Test Sequences and Partial Unmixing Using Multi Sensor Remote Sensing Data. Ph.D. Thesis, Technical University Vienna, Vienna, Austria, 2005, p.199.
48. Hecker, C.; Kuenzer, C.; Zhang, J. Remote-sensing-based coal-fire detection with low-resolution MODIS data. *Rev. in Eng. Geol.*, **2007**, *18*, 229–239.
49. Zhang, J.; Kuenzer, C. Thermal surface characteristics of coal fires 1 results of *in-situ* measurements. *J. Appl. Geophys.* **2007**, *63*, 117–134.
50. Wessling, S.; Kuenzer, C.; Kessels, W.; Wuttke, M.W. Numerical modeling for analyzing thermal surface anomalies induced by underground coal fires. *Int. J. Coal Geol.* **2008**, *74*, 175–184.
51. Li, Z.-L.; Wu, H.; Wang, N.; Qiu, S.; Sobrino, J.A.; Wan, Z.; Tang, B.-H.; Yan, G. Land surface emissivity retrieval from satellite data. *Int. J. Remote Sens.* **2012**, *34*, 3084–3127.
52. Li, Z.-L.; Tang, B.-H.; Wu, H.; Ren, H.; Yan, G.; Wan, Z.; Trigo, I.F.; Sobrino, J.A. Satellite-derived land surface temperature: CURRENT status and perspectives. *Remote Sens. Environ.* **2013**, *131*, 14–37.
53. Sobrino, J.A.; Oltra-Carrió, R.; Sòria, G.; Jiménez-Muñoz, J.C.; Franch, B.; Hidalgo, V.; Mattar, C.; Julien, Y.; Cuenca, J.; Romaguera, M. Evaluation of the surface urban heat island effect in the city of Madrid by thermal remote sensing. *Int. J. Remote Sens.* **2013**, *34*, 3177–3192.
54. Yang, B.; Chen, Y.; Li, J.; Gong, A.; Kuenzer, C.; Zhang, J. Simple normalization of multi-temporal thermal IR data and applied research, on the monitoring of typical coal fires in northern China. In Proceedings of the Geoscience and Remot Sensing Symposium (IGARSS), Seoul, South Korea, 25–29 July 2005; p.5725–5728.

55. Prakash, A. Remote Sensing-GIS Based Geoenvironmental Studies in Jharia Coalfield, India, with Special Reference to Coalmine Fires. Ph.D. Thesis, University of Roorkee, Roorkee, India, 1996.
56. Prakash, A.; Gupta, R.P.; Saraf, A.K. A Landsat TM based comparative study of surface and subsurface fires in the Jharia coalfield, India. *Int. J. Remote Sens.* **1997**, *18*, 2463–2469.
57. Prakash, A.; Gupta, R.P. Land-use mapping and change detection in a coal mining area—Case study in the Jharia coalfield, India. *Int. J. Remote Sens.* **1998**, *19*, 391–410.
58. Prakash, A.; Gupta, R.P. Surface fires in Jharia coalfield, India—Their distribution and estimation of area and temperature from TM data. *Int. J. Remote Sens.* **1999**, *20*, 1935–1946.
59. Dozier, J. A method for satellite identification of surface temperature fields of subpixel resolution. *Remote Sens. Environ.* **1981**, *11*, 221–229.
60. Prakash, A.; Schaefer, K.; Witte, W.K.; Collins, K.; Gens, R.; Goyette, M.P. A remote sensing and GIS based investigation of a boreal forest coal fire. *Int. J. Coal Geol.* **2011**, *86*, 79–86.
61. Sobrino, J.A.; Raissouni, N. Toward remote sensing methods for land cover dynamic monitoring: Application to Morocco. *Int. J. Remote Sens.* **2000**, *21*, 353–366.
62. Gillespie, A.; Rokugawa, S.; Matsunaga, T.; Cothern, J.S.; Hook, S.; Kahle, A.B. A temperature and emissivity separation algorithm for Advanced Spaceborne Thermal Emission and Reflection Radiometer (ASTER) images. *IEEE Trans. Geosci. Remote Sens.* **1998**, *36*, 1113–1126.
63. Gillespie, A.R.; Rokugawa, S.; Hook, S.J.; Matsunaga, T.; Kahle, A.B. *Temperature/Emissivity Separation Algorithm Theoretical Basis Document, Version 2.4*; ATBD Contract NAS5-31372; National Aeronautics and Space Administration: Washington, DC, USA, 1999.
64. Markham, B.; Baker, J. *EOSAT Landsat Technical Notes No. 1*; EOSAT: Lanham, MD, USA, 1986; p. 8.
65. Prakash, A.; Saraf, A.K.; Gupta, R.P.; Dutta, M.; Sundaram, R.M. Surface thermal anomalies associated with underground fires in Jharia coal mines, India. *Int. J. Remote Sens.* **1995**, *16*, 2105–2109.
66. Wang, C. Detection of Coal Fires in Xinjiang (China) Using Remote Sensing Techniques. Master's Thesis, Faculty of Geo-Information Science and Earth Information (ITC), Enschede, The Nethelands, 2002; p. 93.
67. Prakash, A.; Gens, R.; Vekerdy, Z. Monitoring coal fires using multi-temporal night-time thermal images in a coalfield in North-West China. *Int. J. Remote Sens.* **1999**, *20*, 2883–2888.
68. Stracher, G.B.; Prakash, A.; Sokol, E.V. *Coal and Peat Fires: A Global Perspective Volume 1: Coal—Geology and Combustion*; Elsevier Science: Amsterdam, The Netherlands, 2010.
69. Raju, A.; Gupta, R.P.; Prakash, A. Delineation of coalfield surface fires by thresholding Landsat TM-7 day-time image data. *Geocarto Int.* **2012**, *28*, 343–363.
70. Kong, B.; Zhou, Z.; Ma, J.; Zhang, G.; Long, X. Study on integrated detecting on the 18th coal fire zone of Wuda Coalfield. *Shenhua Sci. Technol.* **2009**, *7*, 8–13. (in Chinese)

© 2015 by the authors; licensee MDPI, Basel, Switzerland. This article is an open access article distributed under the terms and conditions of the Creative Commons Attribution license (http://creativecommons.org/licenses/by/3.0/).